

# Understanding Roles of Oceanic Fine Structures in Climate and Its Variability III

Project Representative

Wataru Ohfuchi

Earth Simulator Center, Japan Agency for Marine-Earth Science and Technology

Authors

Hideharu Sasaki<sup>\*1</sup>, Bunmei Taguchi<sup>\*1</sup>, Masami Nonaka<sup>\*2</sup>, Mayumi K. Yoshioka<sup>\*3</sup>,  
Hidenori Aiki<sup>\*2</sup> and Wataru Ohfuchi<sup>\*1</sup>

\*1 Earth Simulator Center, Japan Agency for Marine-Earth Science and Technology

\*2 Research Institute for Global Change, Japan Agency for Marine-Earth Science and Technology

\*3 Hydrospheric Atmospheric Research Center, Nagoya University

We have been investigating air-sea interaction where oceanic structures of small spatial scale play important roles by using high-resolution, primitive equation based, global atmosphere, ocean and coupled models, and a regional non-hydrostatic ocean-atmosphere coupled model. In this report, we present the following four topics: 1) Interannual-to-decadal variability of the sea ice extent in Okhotsk Sea and its associated atmospheric variability, 2) Dynamical feedback in local air-sea interaction along the Hawaiian Lee Countercurrent, 3) Influence of the ocean through sea surface temperature on typhoon intensity, and 4) Predictability of the Kuroshio Extension jet speed.

**Keywords:** air-sea interaction, oceanic front, air-sea coupled simulation, the Okhotsk Sea, Hawaiian Lee Countercurrent, typhoon, Kuroshio Extension

## 1. Introduction

We have been studying relatively small spatial scale interaction of the atmosphere and ocean. In this report, we present a role of air-sea and air-sea-ice interactions in the climate and its variations where oceanic structures of small spatial scale play important roles. Section 2 and 3 present studies using CFES, the ocean-atmosphere coupled general circulation model (GCM) for the Earth Simulator (ES). In Section 2, influences of sea ice variability in the Okhotsk Sea on the climate variations are introduced. Local air-sea interactions induced by the sea surface temperature (SST) maximum along the Hawaiian Lee Countercurrent are presented in Section 3. In Section 4, we also report a study using CReSS-NHOES, Cloud Resolving Storm Simulator-Non-Hydrostatic Ocean model for the ES. Influences of SST on the typhoon intensity are revealed. In Section 5, the predictability of Kuroshio Extension jet speed associated with meridionally-confined frontal-scale variability is suggested using OFES, the ocean GCM for the ES.

## 2. Interannual-to-decadal variability of the sea ice extent in Okhotsk Sea

Sea ice variability has been recognized as an important element of climate system, yet simulating it in climate models is not necessarily successful. Here we focus on the Okhotsk Sea, which is a marginal sea residing just to the north of Japan and is

also the southernmost region of the seasonal sea ice formation regions in the Northern Hemisphere. We investigate the sea ice variability in the Okhotsk Sea and its associated atmospheric variability, using a 120-year CFES simulation integrated at a medium resolutions where the atmospheric component has a horizontal resolution of T119 spectral truncation with 48 vertical  $\sigma$ -levels and the ocean component has 0.5° latitude-longitude grids with 54 z-coordinate vertical levels. The CFES integration exhibits prominent interannual-to-decadal variability in the sea ice extent in the Okhotsk Sea (red curve in Fig. 1a). The analysis of the cause and effect of the simulated sea ice variability confirms that the CFES simulates realistic interactions among the ocean, the sea ice, and the atmosphere. Namely, the larger than normal sea ice extent in the Okhotsk Sea in December tends to be preceded by colder than normal air temperature over the far-east Eurasian region in November (blue curves in Figs. 1a and 1b), and also tends to be followed by the deeper than normal Aleutian low (Fig. 1a gray bar charts, Fig. 1c) leading to the colder air temperature in the northern Japan (not shown) in February. The former atmospheric anomalies in November can be regarded as the forcing for the sea ice variation in the Okhotsk Sea, while the latter atmospheric anomalies in February as an response to the sea ice variation, both of which are consistent with the earlier studies based on observations.

A further analysis reveals that the cold air temperature

anomalies in November is associated with larger than normal sea ice extent in Arctic Sea off East Siberia from September to November (not shown). This link of sea ice variability between the summer-to-fall Arctic Sea and the early winter Okhotsk Sea, which is suggested by the model, is also confirmed with observations, providing an important basis for the seasonal prediction in the areas surrounding the Okhotsk Sea including the Northern Japan.

### 3. Local dynamical feedback into the Hawaiian Lee Countercurrent

Air-sea interactions not only in the tropics but also in the mid-latitude region are of great interest to researchers. The Hawaiian Lee Countercurrent (HLCC), in which the high SST along the HLCC may generate local air-sea interactions, is one example outside the tropics. The HLCC is a narrow eastward countercurrent extending from Hawaii over the date line, which is driven by an orographic wind wake behind Hawaii. The satellite observations revealed atmospheric response with surface wind convergence and high cloud water over the warm HLCC [1]. However, the local air-sea interactions over the HLCC have not been well understood.

In order to examine the local air sea interaction induced by the high SST along the HLCC, we use a medium resolution

version of CFES (as the one used in Section 2). The CFES control run demonstrates the HLCC with high SST band and the atmospheric response to the high SST (Fig. 2). Comparing with a sensitivity simulation reducing an influence of the high SST on the atmosphere by smoothing the SST around the HLCC, air-sea interaction induced by the high SST is investigated with focus on the local dynamical feedback into the ocean. The HLCC speed is higher in the control simulation than that in the sensitivity simulation (Fig. 3), suggesting that dynamical feedback to the ocean following the atmospheric response to the high SST further drives the HLCC with distinct increase of current speed in the south of the HLCC. Both Ekman suction induced by positive wind curl along the surface wind convergence band and eastward Ekman flow induced by northerly wind south of the HLCC axis play roles in the increase of the HLCC speed. In addition, the HLCC speed increase advects warm water from the west, and causes SST warming locally around the HLCC (not shown). When the HLCC speed is high, the high SST band and atmospheric response are distinct. If following dynamical feedback of the HLCC speed increase is further enhanced, the HLCC variations with both seasonal and interannual time scales become more amplified.

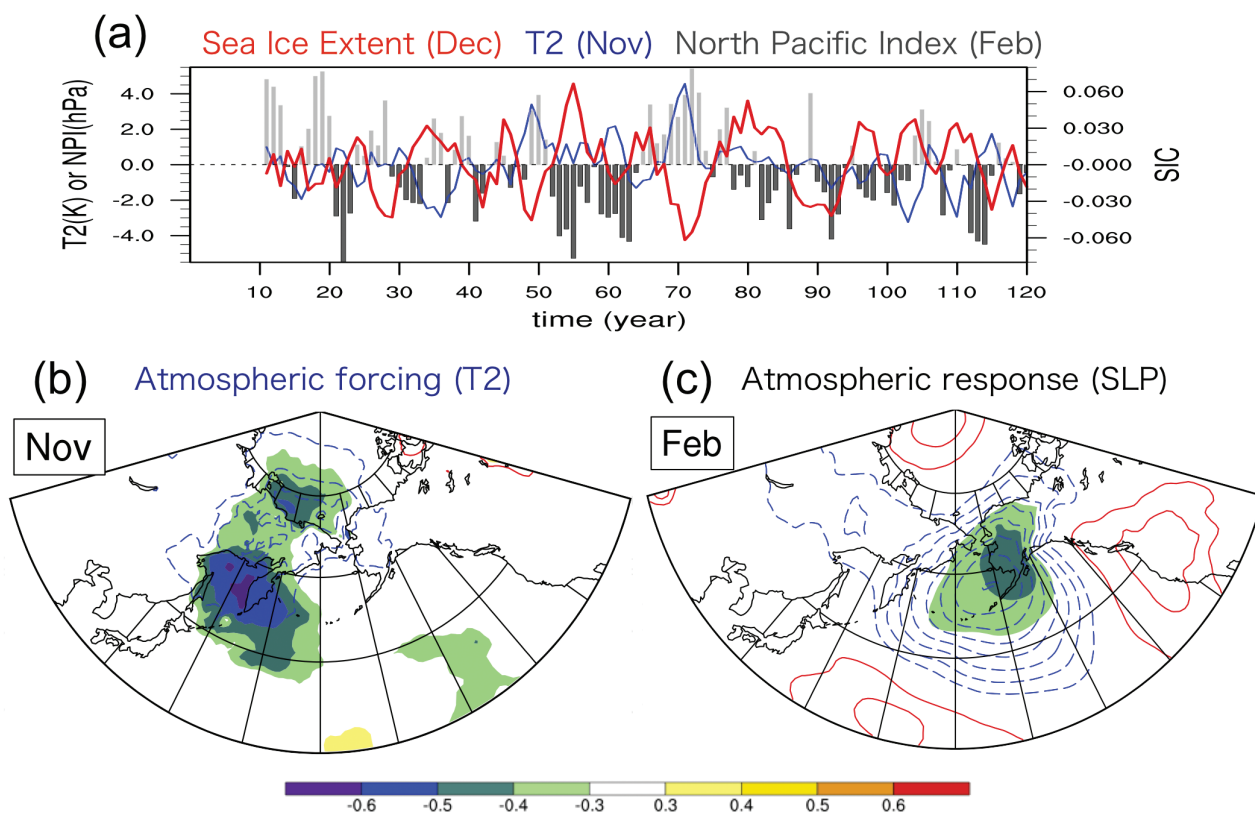


Fig. 1 (a) Time series of sea ice extent averaged over the Okhotsk Sea in December (red), 2-m air temperature averaged over the North East Eurasia (blue), and North Pacific Index (sea level pressure averaged over the central North Pacific; gray bar charts). All the quantities are based on the 120-year CFES integration with 3-year running mean applied after the trend and climatological monthly mean are removed. (b) Lag correlation (color shade) and regression (contours; the interval is 0.2 K) of 2-m air temperature in November onto the area-averaged Okhotsk sea ice variability in December. (c) As in (b) but for sea level pressure in February (contour interval is 2hPa).

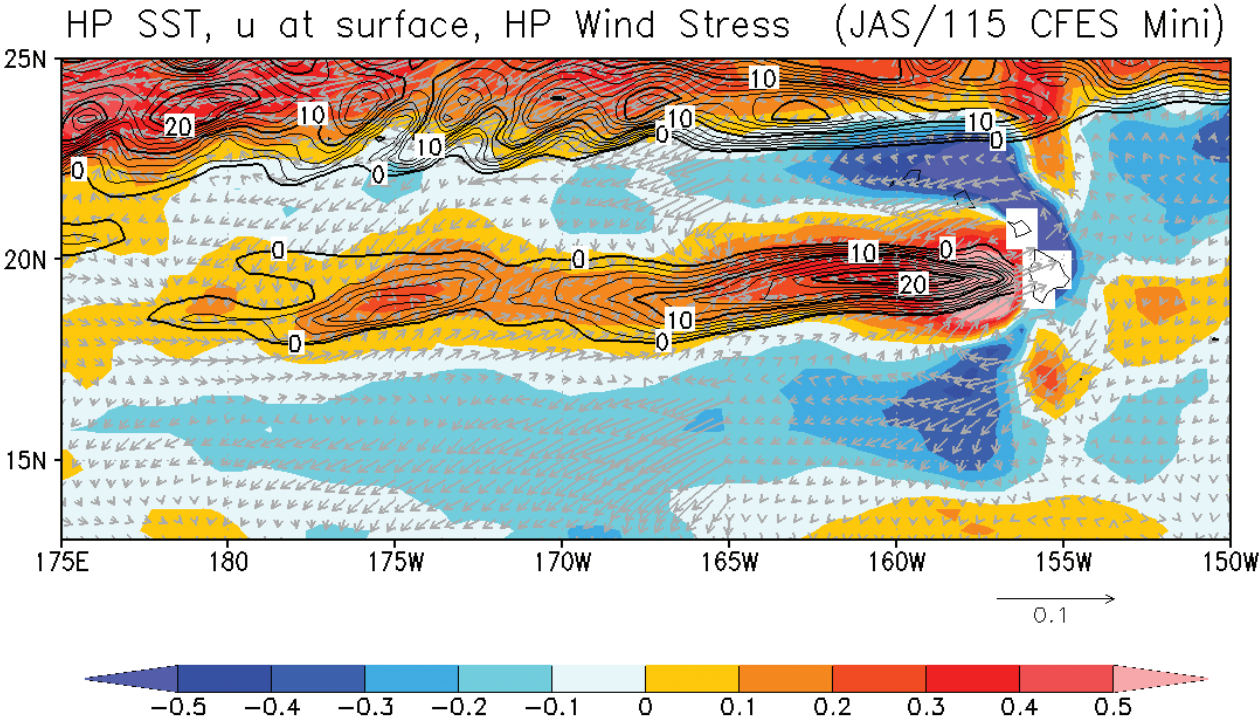


Fig. 2 Geostrophic eastward current speed (contour, cm s<sup>-1</sup>), SST (color, °C) and wind stress vectors (10<sup>-1</sup> N m<sup>-2</sup>) averaged from July to September in the 115th year in the CFES control simulation. Meridional high-pass filter via removing an 8° moving mean is applied to SST and wind stress. Contour intervals are 2 cm s<sup>-1</sup>. Scale of wind stress vectors east of 165°W is ten times that west of 165°W.

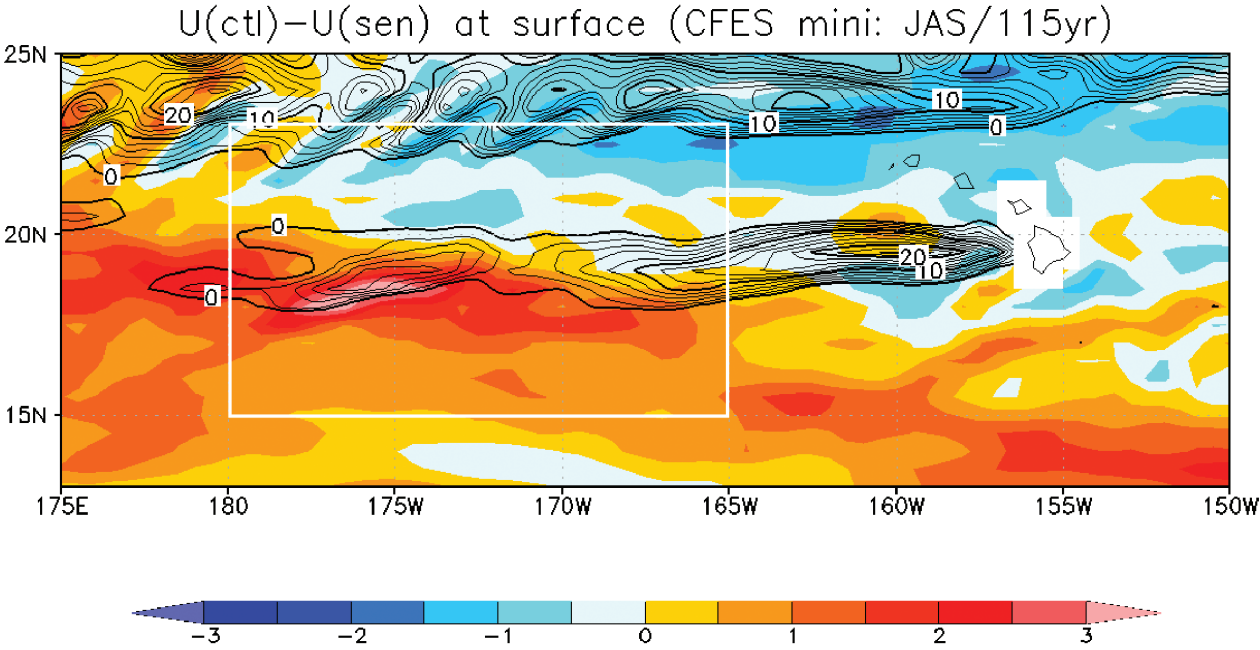


Fig. 3 Eastward surface current speed (cm s<sup>-1</sup>) in the control simulation minus those in the sensitivity simulation averaged from July to September in the 115th year. Contours indicate eastward current speed in the control simulation. Contour intervals are 2 cm s<sup>-1</sup>. In the white box, SST is smoothed in the sensitivity simulation.

#### 4. Influence of the ocean through SST on typhoon intensity

Local distribution of the SST decrease is observed around and after a typhoon's passing (e.g. [2]). The SST decreases remarkably when a typhoon moves at slow speed [3]. On the other hand, the cool SST produced by the typhoon's passing affects the intensity of the typhoon itself, through decrease of the sensible/latent heat flux from the ocean surface by air-sea interaction.

Numerical simulations were performed to investigate intensity change through air-sea interaction for the typhoon Roke (T1115) which was generated at September 10 in 2011 and moved almost stationary around eastern off Okinawa Island during September 16-19 after moving very slowly in the north western Pacific. Experiments were designed with utilizing different sea surface conditions, employed 1) non-coupled ocean (fixed SST), 2) coupled one-dimensional ocean which treats upper layers of the ocean of 30m depth (slab-ocean) and 3) coupled three-dimensional ocean, respectively.

CReSS was utilized for the atmospheric model for all experiments. For three-dimensional experiment, CReSS-NHOES was utilized for the coupled experiment. For initial/boundary conditions, JMA/GPV dataset was employed for the atmosphere and JCOPE2 reanalysis dataset was for the ocean. Numerical experiments were performed for 8-days of the horizontal resolution at 4 km in 21°N-41°N, 122°E-142°E latitudinal -longitudinal domain.

In the experiments, Roke was successfully simulated in staying near Okinawa Island during 16-19. Remarkable difference of the intensity of the typhoon appeared in the central pressure after 60 hours of the integration time among the

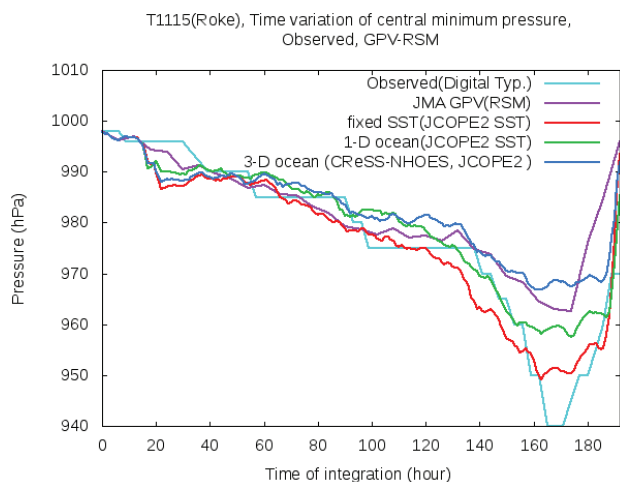
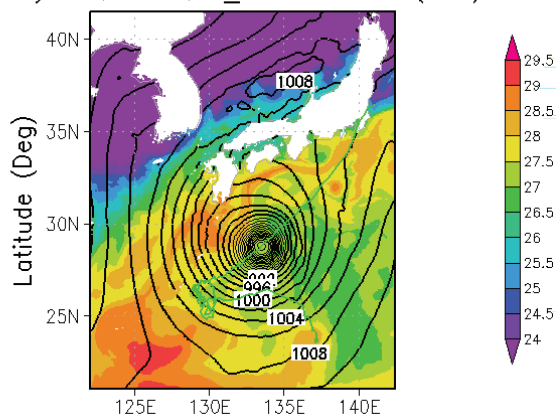


Fig. 4 Time variation of the central pressure simulated for T1115 (Roke). The abscissa is the integration time started from the integration in September 14 00Z. The red line is for the fixed-SST, the green line is for the slab-ocean and the blue is for the CReSS-NHOES coupled experiments, respectively. The values derived from JMA/GPV data and from observation are also plotted with the light blue and purple lines, respectively.

experiments and then was clear after about 80 hours. After about 150 hours, the central pressure in the coupled experiments was higher than that in the fixed SST experiment, of about 10 hPa for slab-ocean experiment and of about 20 hPa for CReSS-NHOES coupled experiment (Fig. 4). The SST distribution of the coupled experiments at September 21 00Z (after 168 hours) are shown in Fig. 5. The cooler SST of 2K appeared in the CReSS-NHOES experiment, which distributed locally in the southwestern part of the Roke's center, where Roke stayed during September 16-19. The warm SST around the Kuroshio currents between Kyushu and Amami islands also decreased in the CReSS-NHOES coupled experiment. At that time, Roke moved to the cooler SST region which generated north-eastern part in Roke's staying. That suggests that three-dimensional response with vertical upwelling and horizontal currents produced by the typhoon Roke induces more SST cooling locally by air-sea interaction than one-dimensional response with vertical mixing only, resulting in more suppression of the central pressure of Roke.

T1115 1Docean Surface Temperature(Deg-C), Day=21,hr=00, P\_Min.=959.475(hPa)



T1115 3Docean Surface Temperature(Deg-C), Day=21,hr=00, P\_Min.=968.694(hPa)

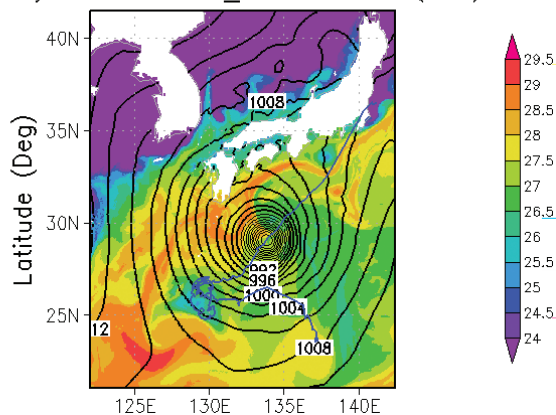


Fig. 5 Snapshot of the SST (colored), the surface pressure (contours), and the tracks of simulated Roke (lines) in the experiments at September 21 00Z : the slab-ocean experiment (upper panel) and the CReSS-NHOES coupled experiment (lower panel), respectively.

Asymmetric SST distribution around the center of the typhoon leads to the regional distribution of the heat flux from the sea surface. Time series of the directional distribution of the heat flux divided the part of north-south/east-west represents the relation between the local SST distribution affected/non-affected by Roke and the location of Roke. Figure 6 shows the time variation of the latent heat flux around the center of Roke averaged within 100 km radius in the experiments. After 120 hours when Roke began to move to north-eastward after staying near Okinawa Island, the flux of the coupled experiments was clearly smaller than that in the non-coupled experiment in the all quadrants, which indicates the suppression of the central pressure shown in Fig. 1. In the northern quadrants after 140 hours of the integration time, the flux of the slab-ocean experiment was greater than that in the CReSS-NHOES coupled experiment. After 150 hours, the flux in of the slab-ocean experiment was as much as that of the fixed-SST experiment and greater than that of the CReSS-NHOES coupled experiment in the north-east quadrant, which indicates that Roke arrived in the region where the ocean was greatly changed in three-dimensionally. In the south-east quadrant, on the other hand, the time varying flux of the slab-ocean experiment is close to

that of the CReSS-NHOES coupled experiment, suggesting less three-dimensional ocean effect in the east off of the Kuroshio currents.

## 5. Predictability of the Kuroshio Extension jet speed

Potential predictability of interannual variability in the Kuroshio Extension (KE) jet speed attributed to the westward propagation of wind-driven oceanic Rossby waves is investigated through prediction experiments with the OFES under the perfect-model assumption.

Though based on the small number of the experiments due to limited computational resources available, our experimental results suggest some predictability not only in broad-scale sea surface height anomalies (SSHAs) but also in anomalous KE jet speed associated with meridionally-confined frontal-scale variability (Figs. 7a and 7b). Specifically, more than half of the variance in the 13-month running mean KE jet speed can be explained by the ensemble mean of the forecast integrations even in the third year (Fig. 7c). The predictability of the KE jet speed thus revealed has been confirmed in the 61-year long hindcast integration as significantly high correlation ( $r =$

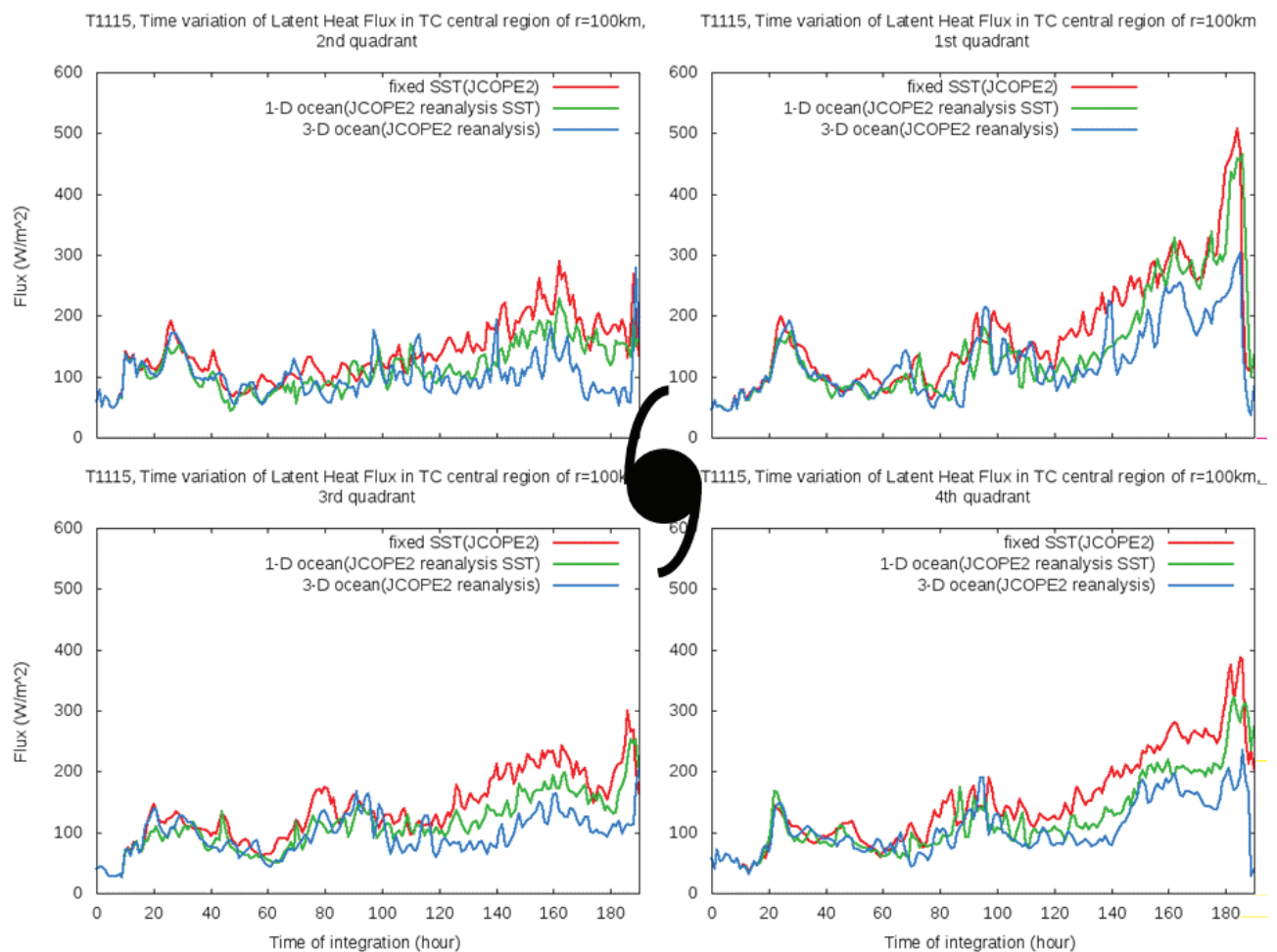


Fig. 6 Time variation of the directional distribution of the latent heat averaged within 100 km around the Roke's center: north-east (upper right), north-west (upper left), south-west (lower left), and south-east (lower right) quadrants, respectively.

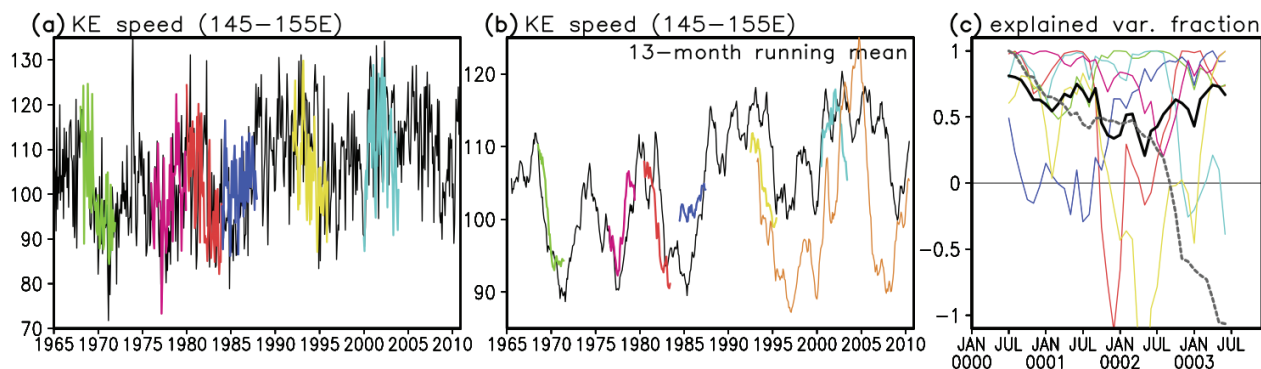


Fig. 7 (a) Time series of the KE jet speed ( $\text{cm sec}^{-1}$ ) averaged over  $[145^{\circ}\text{-}155^{\circ}\text{E}]$ , based on the OFES hindcast integration (black) and six forecast experiments (colors). (b) Same as (a), but 13-month running mean is applied to reduce influences of eddies. Orange curve is for the observed value. (c) Time series of the corresponding fraction of variance explained by the forecast experiments represented by  $1 - (\text{forecast errors})^2 / (\text{signal variance})$  in the KE jet speed in (b). Thick black curve is for the ensemble mean, and grey is for the persistence.

0.68) between the smoothed interannual variability in KE jet speed and SSHAs over the central North Pacific  $[30^{\circ}\text{-}34^{\circ}\text{N}, 170^{\circ}\text{E}\text{-}175^{\circ}\text{W}]$  three years earlier (figure not shown). Though limited in their availability, the satellite observed SSHA data and the geostrophically derived KE jet speed are also correlated if the same time lag is assigned.

Recent studies have suggested that decadal changes in the speed of the Kuroshio and an upstream portion of KE can influence natural mortality of infant Japanese sardine, which is known to yield several orders of interdecadal variability in its mass. Prediction of the path and intensity of KE is thus of social and scientific importance.

## 6. Conclusion

We briefly reported research activities to investigate roles of small-scale oceanic structures in climate and its variability by using simulation results of hydrostatic and non-hydrostatic atmosphere, ocean coupled models. This year, we have concentrated on not only air-sea but also air-sea-ice interactions in the subtropical and subarctic regions. We will study more on interactions between small and large scales and their influence on large-scale climate in the near future.

## References

- [1] S.-P. Xie, W. T. Liu, Q. Liu, and M. Nonaka, "Far-reaching effects of the Hawaiian Islands on the Pacific ocean-atmosphere system", *Science*, 292, 2057–2060, 2001.
- [2] J. F. Price, "Upper ocean response to a hurricane", *Journal of Physical Oceanography*, 11, 153–175, 1981.
- [3] M. A. Bender, I. Ginis, and Y. Kurihara, "Numerical simulations of tropical cyclone-ocean interaction with a high-resolution coupled model", *Journal of Geophysical Research*, 98, 23, 245–23, 263, 1993.

# 海洋微細構造が生み出す気候形成・変動メカニズムの解明

プロジェクト責任者

大淵 濟 海洋研究開発機構 地球シミュレータセンター

著者

佐々木英治<sup>\*1</sup>, 田口 文明<sup>\*1</sup>, 野中 正見<sup>\*2</sup>, 吉岡真由美<sup>\*3</sup>, 相木 秀則<sup>\*2</sup>, 大淵 濟<sup>\*1</sup>

\*1 海洋研究開発機構 地球シミュレータセンター

\*2 海洋研究開発機構 地球環境変動領域

\*3 名古屋大学 地球水循環研究センター

高解像度のプリミティブ方程式と非静力学の全球、または領域の大気、海洋、結合モデルを用いて、海洋の空間的に小さいスケールが重要な役割をはたす大気海洋結合作用を研究している。この報告書では、次の四つの研究成果を取り上げた。全球大気海洋結合モデル CFES を用い、1) 環オホーツク海域における大気海洋海氷相互作用の十年規模変動、2) ハワイ風下反流に伴う大気海洋相互作用の海への力学的フィードバックを明らかにし、3) 非静力学の領域大気海洋結合モデル CReSS-NHOES を用い海面水温の台風強度への影響メカニズムを明らかにした。また、4) 準全球海洋モデル OFES の中で黒潮統流の流速の予測可能性を示した。

キーワード: 大気・海洋相互作用, 海洋前線, 大気海洋結合シミュレーション, オホーツク海, ハワイ風下反流, 台風, 黒潮統流